Scattering, loss, and gain of surface plasmons

Beijnum, F. van

Surface plasmon lasing observed in metal hole arrays

Surface plasmons in metal hole arrays have been studied extensively in the context of extraordinary optical transmission, but so far these arrays have not been studied as resonators for surface plasmon lasing. We experimentally study a metal hole array with a semiconductor (InGaAs) gain layer placed in close (20 nm) proximity of the metal hole array. As a function of increasing pump power we observe an intense and spectrally narrow peak, with a clear threshold. This laser emission is donut shaped and radially polarized. Three experimental observations support that the system shows surface plasmon lasing. First, the full wavelength dispersion of the observed resonances can be understood using a single surface plasmon mode of the system. Second, the polarization of these resonances is as expected for surface plasmons. Third, the magnitude of the avoided crossing, which results from mode coupling at the holes, has a similar magnitude as found in simulations using surface plasmons.

F. van Beijnum, P. J. van Veldhoven, E. J. Geluk, M. J. A. de Dood, G. W. 't Hooft, and M. P. van Exter, submitted for publication.

7.1 Introduction

Surface plasmon lasers and spasers [96] have recently attracted much interest (see e.g. [97] for a review) and are attractive candidates for nanoscale lasers. Lasing is reported in different nanoscale resonators: metal-coated nanopillars [11], metal-coated nanorings [110], semiconductor nanowires on a silver film [40, 111], and gold nano spheres [12]. However, claims of surface plasmon lasing are often hard to substantiate and experimental observations can be misinterpreted as (surface plasmon) lasing [112]. Therefore, studying surface plasmon lasing in a simple and well known model system will contribute to our understanding of surface plasmon lasing and the limitations thereof.

A metal hole array is a thoroughly studied plasmonic system, mainly in the context of extraordinary optical transmission [28]. For surface plasmon lasing, however, hole arrays have not yet been considered. Nonetheless, experiments on hole arrays without a gain material suggest that the holes in the array could provide the required feedback for lasing. For example, the wavelength dispersion of the resonant transmission reveals that the surface plasmons couple with the array, which results in an avoided crossing [28, 49, 50, 113]. This coupling behavior can be related to transmission and reflection coefficients of surface plasmons, using a recently developed [36] and experimentally verified [37] microscopic theory.

More generally, it is shown that two-dimensional photonic crystals with gain can show laser action [114–116]. In the far-infrared a photonic crystal laser is demonstrated where the mode volume is reduced using a surface

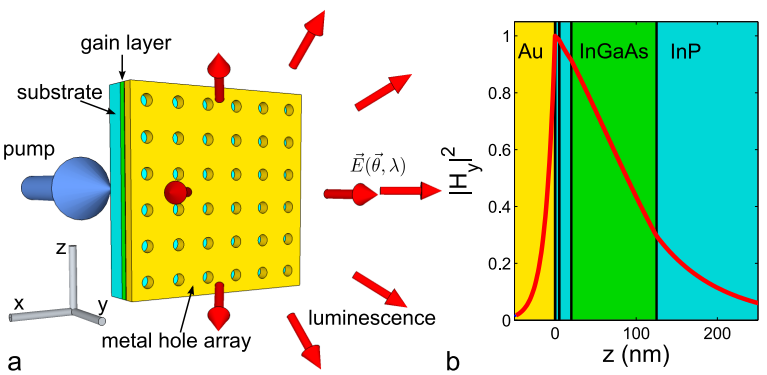

Figure 7.1: a, Sketch of our experiment: a semiconductor layer, in close proximity of a metal hole array, is pumped optically. We perform an angle-resolved study of the luminescence transmitted through the hole array. **b,** The absolute value squared of the magnetic field H_y of the designed surface plasmon mode (solid curve) exhibits a field maximum on the gold-dielectric interface. The 105 nm InGaAs gain layer is placed roughly $20\ \mathrm{nm}$ from the gold, using a InP and SiN spacer layers.

plasmon mode [117]. At these wavelengths, however, the surface plasmon absorption is modest [97]. Hence, a major challenge to obtain lasing in metal hole arrays at optical frequencies is to overcome both the absorption losses and the radiative losses of the surface plasmons.

In this Chapter we demonstrate surface plasmon lasing in metal holes arrays and substantiate our claim of surface plasmon lasing with three different experimental observations. The experiment, illustrated in Fig. 7.1a, studies an optically pumped semiconductor gain layer placed in close proximity of a metal hole array. The luminescence that is transmitted through the hole array is recorded. After discussing this experiment in more detail, we first present the observation of laser action in this system. Thereafter we present measurements on the luminescence that are resolved by angle, wavelength and polarization thereby revealing the nature of the laser action.

7.2 Experiment

In Fig. 7.1b we show the layer stack used in our experiment. On a semi-insulating indium phosphide (InP) wafer a lattice-matched indium gallium arsenide (InGaAs) layer is grown, which is subsequently covered with a thin (15 nm) layer of InP. Hereafter a 5 nm protective silicon nitride (SiN) layer is grown using plasma enhanced chemical vapor deposition. On these layers we fabricate the metal hole array by depositing 100 nm gold and 20 nm titanium on a lithographically defined array of dielectric pillars. To provide sufficient adhesion of the gold onto the SiN, we deposit a very thin (average thickness smaller than 0.5 nm) titanium adhesion layer in between these layers. The last step is to etch the pillars away, leaving the subwavelength holes (diameter 160 nm).

To estimate the gain required to compensate the absorption loss of the surface plasmons, we calculate the complex effective refractive index of the layer structure numerically [88]. The spatial mode overlap between the gain layer and the surface plasmon is shown in Fig. 7.1b, solid red curve. Using literature values for the complex refractive index of the gold, InP and InGaAs layers and a measured value of the SiN layer, we find that a material gain of 3×10^3 cm^{-1} is required to compensate the absorption loss of the surface plasmon mode. This required gain is large, but realistic for bulk InGaAs [109].

The real part of the calculated effective refractive index is closely related to the wavelength of the resonances in a metal hole array [36, 37]. For the 105 nm InGaAs layer the surface plasmon has a calculated effective refractive index of $n_{\text{eff}} = 3.43$. The InGaAs layer thickness is chosen to maximize the gain, while maintaining single mode operation. For our system the transverse electric waveguide mode is well below cut-off, as this mode is only supported

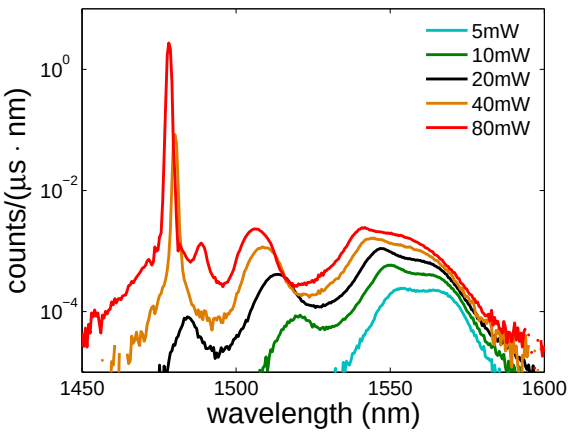

Figure 7.2: Luminescence spectra as a function of pump power, plotted on a semilog scale. For increasing pump power the bandwidth of the luminescence increases until the device starts lasing. Above threshold, the emission of the non-lasing resonances starts to saturate at a maximum intensity.

for InGaAs thicknesses above ~ 170 nm.

Our experimental setup is as follows. We pump the InGaAs gain layer using a continuous wave laser at a wavelength of 1064 nm. To pump the structure with a uniform intensity we illuminate a 600 μm diameter pinhole with the gaussian laser beam, and image this aperture on the sample with a 20x demagnification. The sample is placed in a Helium flow cryostat to study the structure at temperatures down to 5 K. The cryostat has windows on both sides of the hole array sample, allowing us to pump the structure on one side and study the luminescence at the other side.

We record the luminescence as a function of the angle $\vec{\theta}$, by imaging (Magnification = 0.25) the Fourier plane of a microscope objective with a long-working-distance (Mitotoyu, focal distance 10 mm, NA=0.4) on a single-mode fiber placed on a xyz-stage. The angular resolution of our setup is approximately 4 mrad, which is determined by the modal-field diameter of the single-mode fiber. By scanning the fiber through the Fourier plane and spectrally resolving the fiber output (~ 1 nm resolution), we can create an image of the Fourier plane for each emitted wavelength. In addition to the far-field imaging, we can also adjust the optics such that the fiber is placed in an image plane of the sample, allowing us to make spatial images of the laser for each wavelength.

7.3 Laser threshold

In Fig. 7.2 we plot the recorded spectra as a function of the pump power, at an angle $(\theta_x, \theta_y) = (0 \text{ mrad}, 48 \text{ mrad})$. For most pump powers three maxima in the luminescence are seen. These maxima are associated with different resonances of the hole array, of which the origin will be discussed later. As the

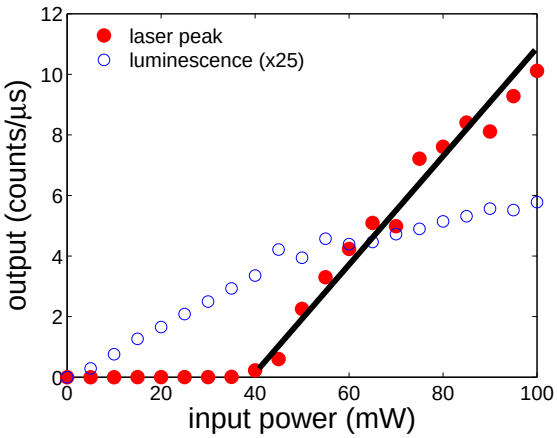

Figure 7.3: The output in the lasing peak and in the luminescence in the range of $1485 - 1600$ nm. The power in the lasing peak shows a clear threshold (red). The black line is a guide to the eye. The luminescence outside the lasing peak starts to level off, as expected for lasing in semiconductor devices (blue).

pump power is increased from 5mW (cyan) to 20mW (black) the luminescence maxima at ~ 1560 nm and ~ 1520 nm increase in intensity, and a third peak becomes visible at ~ 1480 nm. Increasing the intensity further to 40 mW (orange) the ~ 1480 nm peak increases dramatically. A further increase in the pump power to 80 mW (red) shows an increase of the ~ 1480 nm peak by more than an order of magnitude, while the intensity of the 1510 nm peak increases only a factor two. The dramatic increase of the ~ 1480 nm peak suggests that the structure is lasing.

The existence of a clear laser threshold is supported by Fig. 7.3, where we plot the recorded intensity integrated over the spectral peak at ~ 1480 nm as a function of input power. A distinct laser threshold is seen at roughly 40 mW pump power. We also plot the integrated luminescent intensity in the wavelength range of $1485 - 1600$ nm. The integrated luminescence first increases linearly with the input power but for powers larger than the threshold it starts to level off, indicating the expected carrier pinning [11, 108].

The results presented in Figs. 7.2 and 7.3 are for a laser that has a lattice spacing of 470 nm, and lases at 1478 nm. We also fabricated lasers with a lattice parameter of 460 nm and 450 nm. Both devices show lasing too, with the laser wavelengths of 1450 nm and 1419 nm respectively. Hence the ratio between the laser wavelength and lattice parameter is a constant, namely 3.15 ± 0.01. This clear relation between the lattice constant and the laser wavelength shows that the hole array is used as a resonator.

7.4 Dispersion

To reveal the origin of the three resonant peaks in Fig. 7.2, we will now study the wavelength dispersion of these resonances. This dispersion has been

intensively studied in the context of the extraordinary optical transmission [28, 49]. In these experiments the resonant wavelength of the transmission is studied as a function of the angle of incidence. We use angle-resolved measurements of the luminescence, below laser threshold, to study the dispersion of the resonances in our structure. A study below threshold is convenient, as it allows us to study the angle-resolved luminescence without a lasing peak that saturates our detector.

The emission angle as a function of wavelength can often be understood using a simple model that assumes uncoupled traveling waves. For two neighboring holes on either the x-axis or y-axis this traveling wave has a phase difference of $k_x a_0$ or $k_y a_0$ respectively, with $\vec{k} = (k_x, k_y)$ the wave vector of the traveling wave. This linear phase results in a plane wave emitted at an angle (θ_x, θ_y). Relating k_x and k_y to the total momentum, $k^2 = k_x^2 + k_y^2$, the emission angle can be calculated [49]:

$$n_{\text{eff}}^2 k_0^2 = |k|^2 = \left|k_{||,x} - m_x G\right|^2 + \left|k_{||,y} - m_y G\right|^2 . \tag{7.1}$$

with $G = 2\pi/a_0$, n_{eff} the mode index of the traveling wave, (m_x, m_y) the diffraction order, $k_{||,x} = k_0 \sin\theta_x$ and $k_{||,y} = k_0 \sin\theta_y$. Equation (7.1) describes a circle of radius k around the point $(m_x G, m_y G)$. In our measurements, the mode index is the only unknown parameter. Equation (7.1) describes uncoupled traveling waves, but often suffices to understand the main features of the dispersion. For the relatively weakly interacting surface plasmons, the avoided crossing can only be observed when curves of different (m_x, m_y) intersect.

In Fig. 7.4 we show the measured angle-resolved luminescence for nine wavelengths, along with a plot of Eq. (7.1) for $n_{\text{eff}} = 3.26$. We plot the images with decreasing wavelength, i.e. increasing k. The general behavior is well predicted by the simple model and shows the square symmetry of the lattice. As a function of k the circles increase in radius, thus move towards the optical axis (1600 nm − 1540 nm), cross it (1540 nm − 1520 nm) and thereafter move away from it (1520 nm − 1440 nm). At the angular position where the theoretical lines intersect, coupling is found (1520 nm − 1440 nm), changing the far field drastically. From the correspondence between the figures and the theory for uncoupled modes we conclude that one value of n_{eff} is required to understand all far-field luminescence patterns. Given that our layer stack only supports a single mode, the surface plasmon, this is the first experimental observation that supports our claim of surface plasmon lasing.

The found value of $n_{\text{eff}} \sim 3.26$ is low compared to the value we expect for the surface plasmon mode (3.43). This difference is partially due to cooling the sample and a carrier induced refractive index change. Furthermore, the

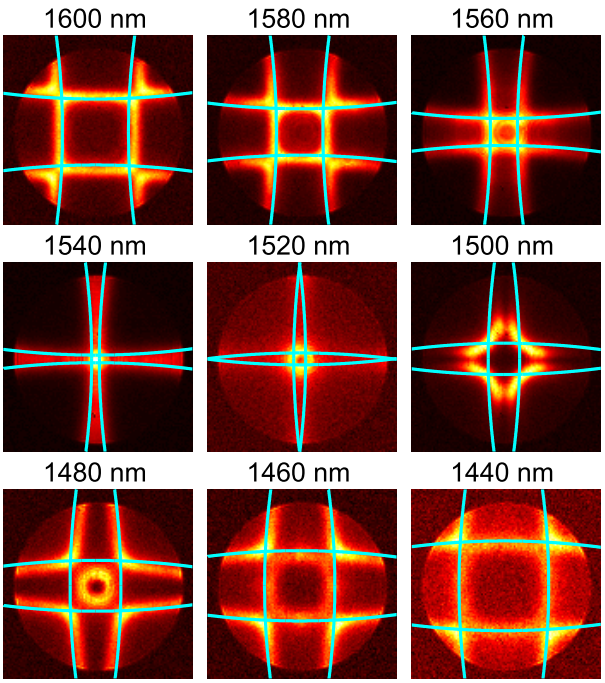

Figure 7.4: Far field emission pattern for nine wavelengths. The device is operated at 150K, where the gain is too small to reach threshold. These images reveal the dispersion of the modes inside the metal hole array. The cyan lines correspond to the dispersion of uncoupled traveling waves with an effective index of 3.26, showing that only one mode is needed to understand the dispersion of the luminescence maxima. The circle shows the numerical aperture of the microscope objective (NA=0.4), the optical axis is the center of this circle.

predicted value of n_{eff} is very sensitive to the thickness of the low-index layer of SiN. Increasing the thickness of this layer 10 nm already lowers the index of the surface plasmon from 3.43 to the experimentally observed value of 3.26. An alternative explanation for the low value of n_{eff} is a thin layer of oxide on the InP.

The luminescence in Fig. 7.4 is recorded without using a polarizer. By studying the dispersion of the resonances for *p*- and *s*-polarization separately, we can show whether the observed resonances are mediated via a transverse electric (TE) or a transverse magnetic (TM) mode [118]. Performing this measurement, we find three *p*-polarized resonances and one *s*-polarized resonance if we scan along θ_y while setting $\theta_x = 0$ (see appendix). The observed polarization dependence of the resonances is consistent with a TM mode around $\lambda/a_0 = n_{\text{eff}}$. Because a surface plasmon is a TM-polarized mode, this provides the second observation that substantiates our claim of surface plasmon lasing.

From this dispersion we can also quantify the magnitude of the coupling that the mode experiences from the holes. As discussed in the appendix the avoided crossing has a splitting of roughly 65 nm, which compares very well with the simulated avoided crossing for surface plasmons (70 nm), while the splitting for a TE mode is less than 1 nm. Hence, the magnitude of the splitting

of the avoided crossing is the third experimental observation that supports a claim of surface plasmon lasing.

7.5 Polarization of laser emission

Last, we find that the laser emission is donut shaped, as shown Fig. 7.5a, which shows the emission above threshold for a temperature set at 5 K. This behavior compares well to transmission experiments and simulations on these hole arrays, where it is shown that this resonance vanishes when excited at normal incidence [36, 107]. The diameter of the ring we observe is 120 mrad, which is Fourier related to a diameter of roughly 16 μm on the sample. The donut shaped emission reproduces in all lasing samples, although the beam quality varies from sample to sample.

To study the local polarization of the lasing mode we show an image of the emission when the vertical polarization is selected using a polarizer (Fig. 7.5b). This image, on the same intensity scale as Fig. 7.5a now shows two lobes, instead of a ring. If we set the polarizer at an arbitrary angle of 30 degrees (Fig. 7.5c) the lobes rotate along with the polarizer, showing that the laser emission is radially polarized. This radial polarization is consistent with the polarization analysis performed in the appendix, which shows that for angles $(0, \theta_y)$ the polarization is vertical and for angle $(\theta_x, 0)$ the polarization is horizontal.

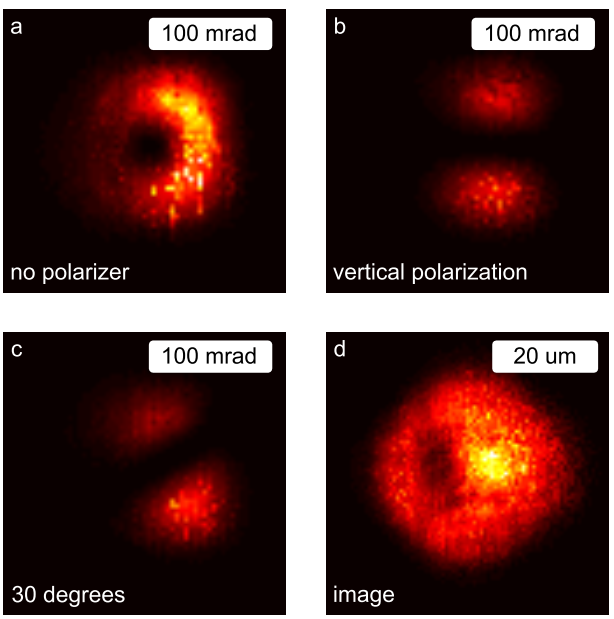

Figure 7.5: **a-c,** Polarization analysis of the angle resolved intensity at the lasing wavelength. **a,** No analyzing polarizer. **b,** Vertical polarization selected. **c,** Thirty degrees from vertical. **d,** Direct image of the luminescence at the lasing wavelength. The structure lases at all positions where it is pumped.

In Fig. 7.5d we also show an real-space image of the laser mode. The round circular spot is comparable to the size of the pumped area (~ 30 μm), albeit somewhat larger (~ 40 μm). This size difference between the lasing spot and pump spot is probably due to carrier diffusion out of the pumped region, which is expected to be a few micrometer. The observed emission is really laser light, as a similar image at a non lasing wavelength is three orders of magnitude less intense. When comparing Figs. 7.5a and 7.5d, we note that the far-field spot is not Fourier related to the image of the lasing spot. This suggests that the laser has multiple spatial modes, a hypothesis that is supported by the observation that we can reduce the size of the pump spot and still obtain lasing.

7.6 Conclusion

We have demonstrated surface plasmon lasing in metal hole arrays. The luminescent input-output characteristic shows clear threshold behavior and the integrated emission levels off, which indicates carrier density pinning [11, 108]. The laser emission is not linearly polarized but radially polarized and thus donut shaped. We find three experimental observations that support our claim of surface plasmon lasing: first, the angle-resolved luminescence shows that all observed resonances are mediated via one mode, while the layer stack only supports a surface plasmon; second, the polarization of the four observed resonances is as expected for surface plasmons; third, the dispersion shows a large avoided crossing of which the magnitude is almost the same as found from simulations using surface plasmons.

Using metal hole arrays as laser resonators could be very important in understanding surface-plasmon lasing, as we consider it to be an ideal model system. The metal hole arrays are well-known structures, hence deviations from the expected behavior can be interpreted in terms of new physical effects induced by the lasing surface plasmon. The metal hole arrays provide the ability to study the band structure and perform polarization analysis, which yields insights into the laser physics. Further miniaturizing the laser, for example by increasing the feedback provided by holes, could make the laser more interesting for photonic integration.

Appendix

In this Appendix we perform a polarization-resolved study of the resonances found in the far-field luminescence, presented in Fig. 7.4. We hereafter compare these measurements to simulations of the angle-dependent transmission of these arrays.

Figure 7.6 shows the measured dispersion of the resonances for p- and s-polarization. These measurements are performed by scanning the fiber along the θ_y direction and at $\theta_x = 0$. We then select either the vertical (corresponding to p) or horizontal (corresponding to s) polarization using a polarizer.

For the p-polarization, we find three resonances. For two of these resonances the emission angle depends linearly on $\sin\theta_y$, except for small angles. This dispersion characteristic is very comparable to that seen in a one dimensional system where TM-polarized traveling waves propagate in the plus or minus y-direction. Close to the optical axis an avoided crossing with a splitting of 65 nm is found. The third resonance seen for the p-polarization shows very little dispersion. In literature it is shown, using two-dimensional coupled mode theory, that such a low dispersion mode is expected for the p-polarization [118]. For the s-polarization, only one resonance is found. Also this low-dispersion resonance is predicted by two-dimensional coupled mode theory [118]. This s-polarized resonance is degenerate on the optical axis with a p-polarized resonance. This polarization dependence has been observed experimentally in several transmission measurements on hole arrays [28, 49, 50, 107, 113]

Although the dispersion of the measured resonances is associated with a TM mode, it is not necessarily a surface plasmon. To study this in more detail, we perform rigorous coupled-wave analysis using commercially available code (Rsoft Diffractmod). This software allows us to simulate the angle-dependent

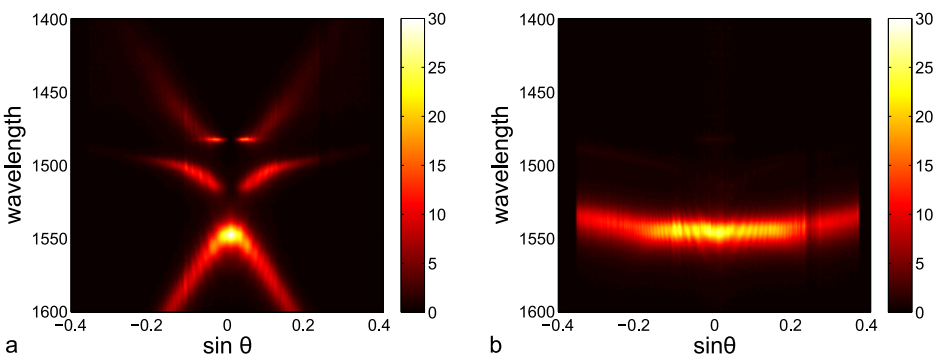

Figure 7.6: Wavelength dispersion of the resonances as a function of the radiation angle $(0, \theta_y)$ for p-polarization (**a**) and s-polarization (**b**). At each non-zero angle we observe three p-polarized resonances and one s-polarized resonance in this wavelength range. The scale bar shows the counts per millisecond.

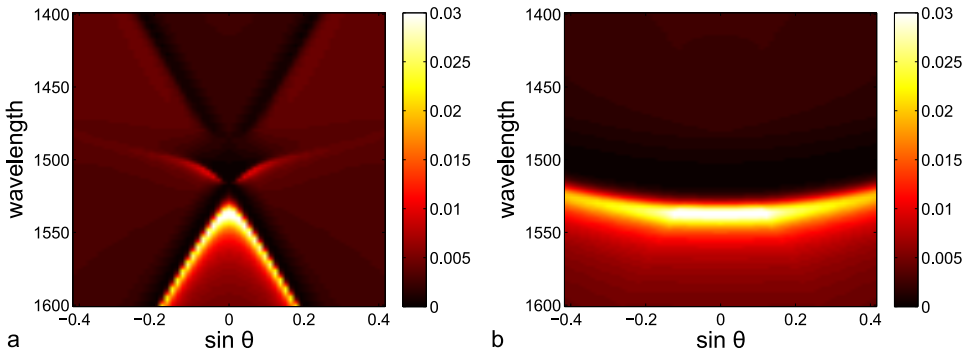

Figure 7.7: Simulated angle dependent transmission spectra for p-polarization (**a**) and s-polarization (**b**). As with the measurements, three resonances are visible for p-polarization at a given angle, and only one for s-polarization. In addition, the splitting found in the simulations is comparable to that found in the experiment.

transmission of the metal hole array with the layer structure that we designed. Using the original design, Fig. 7.1, we found that the resonance is shifted with respect to the observed resonance wavelengths. From the dispersion data presented in the main manuscript we already concluded that if the lasing is mediated via surface plasmons, their effective index is lower than anticipated.

As discussed in the main manuscript, the measured effective refractive index of the surface plasmon does not the match the expected value. To shift the simulated resonance wavelength to that of the measurement we replaced the SiN layer with a 15 nm layer with an index of 1.8, which shifts the transmission resonance close to the observed luminescence maximum. The gain layer is set to have a gain of 3000 cm^{-1}. For this simulation, the effective mode index of the surface plasmon mode that exists on the metal-dielectric interface is calculated to be $n_{\mathrm{eff}} = 3.21$.

The simulated angle-dependent transmission is presented in Fig. 7.7, where Fig. 7.7a shows the p-polarization, and Fig. 7.7b shows the s-polarization. The product of the mode index ($n_{\mathrm{eff}} = 3.21$) and the lattice parameter (470 nm) is 1510 nm, which is roughly in the center of the avoided crossing. In contrast to the luminescence, this angle-dependent transmission contains a Fano resonance, because there is interference between light that is directly transmitted through the hole and light transmitted via surface plasmons.

Two important observations can be made from the comparison between the simulated resonances and the measurements. First, both the simulation and measurement shows that the system has three p-polarized resonances and one s-polarized resonance. Second, the magnitude of the splitting ($\sim$ 70 nm) simulated for p-polarization agrees reasonably well to that of the measurements ($\sim$ 65 nm). Hence, the measured dispersion appears to be a signature of

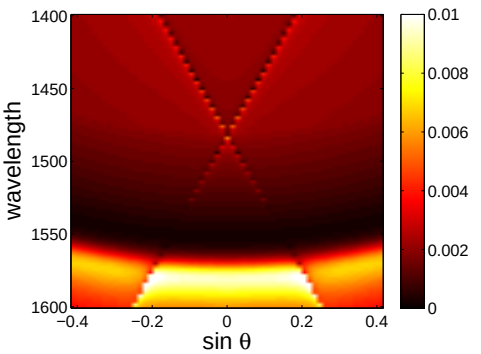

Figure 7.8: Simulated angle-dependent transmission spectra for a TE mode, simulated for s-polarization. Most importantly, the splitting on the optical axis is practically negligible for this mode.

surface plasmons. This is additional evidence that the lasing is mediated via surface plasmons.

To be sure that the splitting and the dispersion is unique for surface plasmons we will now introduce another mode by increasing the InGaAs from 105 nm to 180 nm thickness. This will introduce a guided TE-mode, and it will increase the effective index of the surface plasmon from 3.21 to 3.30. Hence, the surface plasmon resonances will be red-shifted by approximately 42 nm. To make the surface plasmon mode less prominent we now set the gain in the InGaAs layer to zero.

In Fig. 7.8 the simulated dispersion for this thicker gain layer is seen, for s-polarization. Three resonances are seen, two narrow resonances that intersect at $\sim$ 1480 nm and one broad resonance at $\sim$ 1580. The broad resonance is the surface plasmon resonance, also seen in Fig. 7.7 for s-polarization, but shifted by the expected 40 nm. The narrow resonances that intersect on the optical axis are mediated via the introduced TE-mode. The resonances are much sharper than for surface plasmons, because the guided mode experiences less absorption loss. The avoided crossing for this TE mode is too small to be observed, showing that a TE mode in our system does not experience strong feedback from the holes.

In conclusion of this appendix, we have shown three aspects of the dispersion that show that we observe a surface plasmon mode in our experiments. First, the measured dispersion corresponds closely to simulations in which we know we are dealing with surface plasmons: three p-polarized resonances are observed and one s-polarized resonance is observed. Second, we extracted the magnitude of the avoided crossing which is almost identical in experiments and simulations. This shows that the avoided crossing has a magnitude that is to be expected for surface plasmons. Finally, we show that a TE mode has a negligible avoided crossing.